Laser spectroscopy of calcium and strontium monoazide free radicals

C. R. Brazier and P. F. Bernath[a)]
Department of Chemistry, University of Arizona, Tucson, Arizona 85721

(Received 2 September 1987; accepted 26 October 1987)

We have synthesized the gas-phase metal azides CaN_3 and SrN_3. These ionic metal monoazides were found to have linear geometries. The positions of the $\tilde{A}\,^2\Pi$–$\tilde{X}\,^2\Sigma^+$ and $\tilde{B}\,^2\Sigma^+$–$\tilde{X}\,^2\Sigma^+$ electronic transitions were determined as well as several vibrational frequencies. The 0–0 band of the $\tilde{A}\,^2\Pi$–$\tilde{X}\,^2\Sigma^+$ system of SrN_3 has been rotationally analyzed by laser excitation spectroscopy yielding a Sr–N bond length of 2.26 Å.

INTRODUCTION

We have recently studied a series of pseudohalide derivatives of the alkaline earth metals calcium and strontium. These include species isoelectronic with the fluorides such as hydroxides,[1–3] amides,[4,5] and methides[6] as well as cyanates[7,8] and cyanides.[9]

Our initial low-resolution observations of calcium and strontium monocyanate[7] (CaNCO and SrNCO) were consistent with linear structures but were inconclusive as to whether the metal was bound to the oxygen (cyanate) or nitrogen (isocyanate) end of the NCO^- group. A major reason for undertaking this study of the azide derivatives of Ca and Sr was for comparison with the cyanate derivatives. If the NCO^- ligand is nitrogen bonded, then the spectrum of SrNCO should be very similar to that of SrNNN and this, indeed, was found to be the case. The full results of the high-resolution analysis of strontium isocyanate and a comparison with strontium monoazide are presented in the following paper.[8]

While no previous gas phase studies of metal azides have been carried out, there have been extensive studies in solution and in the solid state. An excellent review of the chemistry of azides is given by Patai[10] and of pseudohalides in general by Golub *et al.*[11] The properties of the inorganic azides are discussed in *Energetic Materials*, edited by Fair and Walker.[12] The pure azide species fall basically into two categories: the ionic azides such as $NaN_3(s)$, which are moderately stable and contain an N_3^- group which is symmetrical and linear; and the covalently bound azides such as ClN_3 which are unstable, frequently explosive, and contain an unsymmetrical N_3 group. The very explosive inorganic azides such as $AgN_3(s)$ and $CuN_3(s)$ are thought to also have considerable covalent character. The covalent azide molecules XNNN, X = H,F,Cl,Br,I,CH_3, etc. have an XNN angle less than 180°. SrNNN, the first gas-phase ionic metal azide to be spectroscopically characterized, has the SrNN angle equal to 180°.

Among the investigations of the solid phase azides are studies of their decomposition,[13–15] electronic structure,[16] vibrational frequencies,[17] and crystal structure[18,19]. These studies show that both $Ca(N_3)_2$ and $Sr(N_3)_2$ are ionic solids, containing a symmetrical linear azide anion.

The free azide anion has recently been studied in the gas phase. The first investigations using ICR (Ref. 20) and electron detachment[21] gave a value for the electron affinity of N_3 of 2.76 eV. The spectroscopic parameters of the gas phase N_3^- molecule have been calculated by Botschwina.[22] Most recently, the infrared vibration–rotation spectrum was observed by Polak *et al.*[23]

We have observed the $\tilde{A}\,^2\Pi$–$\tilde{X}\,^2\Sigma^+$ and $\tilde{B}\,^2\Sigma^+$–$\tilde{X}\,^2\Sigma^+$ transitions of CaN_3 and SrN_3 free radicals and determined several vibrational frequencies. In addition, the 0–0 band of the $\tilde{A}\,^2\Pi$–$\tilde{X}\,^2\Sigma^+$ transition of SrN_3 has been studied at rotational resolution and the spectroscopic parameters determined.

EXPERIMENTAL

Calcium and strontium azides were produced in a Broida-type oven[24] by the reaction of the metal vapor with hydrogen azide gas. The solid metal was resistively heated in an alumina crucible and entrained in a flow of argon carrier gas. Typical pressures were about 1 Torr of Ar and a few mTorr of HN_3.

Hydrogen azide was produced by the reaction of sodium azide with molten stearic acid[25] and flowed continuously into the oven. A pressure of a few Torr of HN_3 was maintained in the 1 l reaction flask in order to provide a steady flow into the oven. Solid, liquid, and gaseous HN_3 are dangerously explosive. HN_3 was never condensed in a trap and the pressure of HN_3 was always kept less than 10 Torr.

The metal vapor reacted strongly with the hydrogen azide producing a bright blue-orange chemiluminescent flame. Following the initial observation of chemiluminescence, laser excitation spectra were recorded. The output from a broadband dye laser (Coherent 599-01, 1 cm^{-1} bandwidth) operated with DCM dye and pumped by a Coherent 90-4 argon ion laser was focused into the oven. The laser-induced fluorescence was detected by a photomultiplier tube with a bandpass filter and lock-in amplifier to discriminate against chemiluminescence. The emission was then focused onto the slits of a 0.64 m monochromator and the dispersed fluorescence spectrum recorded using a cooled photomultiplier tube (RCA C31034) and photon counting electronics.

To complete the analysis a high resolution spectrum of the 0–0 band of the $\tilde{A}\,^2\Pi$–$\tilde{X}\,^2\Sigma^+$ transition of SrN_3 was recorded. For this experiment the broadband laser was replaced by a single frequency computer-controlled Coherent 699-29 ring dye laser. Spectra were recorded by scanning the laser and monitoring the fluorescence resolved through the monochromator. The monochromator acted as a narrow

[a)] Alfred P. Sloan Fellow.

 0021-9606/88/042112-05$02.10

bandpass filter to select out the 0–0 band lines from the strong background of lines from other vibrational bands. This also facilitated the rotational assignment as the monochromator could be narrowed to observe fluorescence from a single rotational line in a given branch and the laser scanned until the single line having a common upper state rotational level was found. Ground state combination differences were then obtained and a rotational assignment was easily achieved.

RESULTS AND DISCUSSION

Low-resolution analysis

When hydrogen azide gas was added to the Broida oven, it reacted with the calcium vapor to produce a bright blue-orange chemiluminescent flame. The light was dispersed through a monochromator and it was found that the blue color arose from ^1P–^1S emission from calcium atoms while the orange light came from several molecular species. The chemiluminescence spectrum is shown in Fig. 1.

The chemiluminescent emission comes from molecules which are vibrationally and rotationally hot. A much clearer spectrum was obtained by scanning a dye laser through this region and monitoring the total fluorescence as shown in Fig. 2. Bands arising from the known species CaOH, $CaNH_2$, and CaH were readily assigned. However, the strongest feature, a doublet near 6150 Å, did not belong to any known molecule so this was tentatively assigned to CaN_3. The splitting between the two peaks is 76 cm^{-1}, characteristic of the spin–orbit interaction for calcium bonded to a linear ligand for the $\tilde{A}\,^2\Pi$–$\tilde{X}\,^2\Sigma^+$ electronic transition.

To obtain information about the vibrational frequencies, the laser was tuned to excite one spin–orbit component and the resultant fluorescence dispersed through the monochromator. The spectrum obtained is shown in Fig. 3. Significant relaxation to the other spin–orbit component is apparent as the unpumped spin component has almost half the intensity of the one directly excited. In addition, emission from the $\tilde{B}\,^2\Sigma^+$–$\tilde{X}\,^2\Sigma^+$ band at 5850 Å can also be seen. These assignments are based on the analogy with other linear calcium-containing species such as CaOH where the $\tilde{A}\,^2\Pi$–$\tilde{X}\,^2\Sigma^+$ (Refs. 26 and 2) transition occurs at 6250 Å

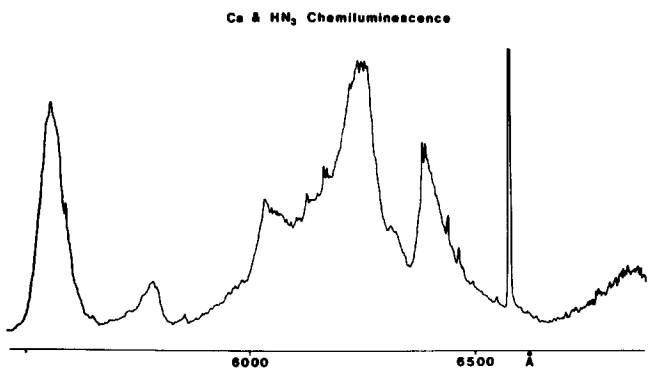

FIG. 1. Chemiluminescent emission from the reaction of calcium vapor with hydrogen azide. The emission arises from four molecular species produced in the flame: CaOH, CaN_3, $CaNH_2$, and CaH. The $^3P_1$–$^1S_0$ atomic line of Ca can also be seen at 6573Å.

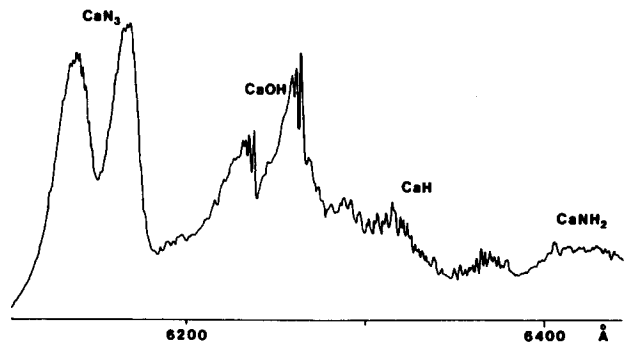

FIG. 2. Laser-induced fluorescence spectrum recorded by scanning the laser and detecting the total fluorescence with a photomultiplier tube. No correction for laser power changes or detector response has been made. Bands due to the four molecular species produced in the flame can clearly be seen.

(as can be seen in Fig. 2) and the $\tilde{B}\,^2\Sigma^+$–$\tilde{X}\,^2\Sigma^+$ transition at 5550 Å (Fig. 1).

The electronic transition is centered on the calcium atom which means that only those vibrations closely associated with the metal are seen strongly. As is typical for these species, the most intense mode is the metal ligand stretch. In this case, emission (3_1^0 band) to $v = 1$ of the Ca–N stretch can be seen 396 cm^{-1} to the red of of the origin band. CaN_3 has five vibrational modes, three stretches, and two degenerate bends: $\nu_1(\sigma)$ the "symmetric" N–N–N stretch, $\nu_2(\sigma)$ the "antisymmetric" N–N–N stretch, $\nu_3(\sigma)$ the Ca–N stretch, $\nu_4(\pi)$ the N–N–N bend, and $\nu_5(\pi)$ the Ca–N–N bend. For the Ca–N stretch (ν_3) the corresponding mode (also ν_3) of $CaNH_2^4$ is at 524 cm^{-1}. If pseudodiatomic reduced masses are computed by assuming that the ligand masses are concentrated at a single point then the vibrational frequency of CaN_3 is predicted to be 392 cm^{-1}. This is further confirmation of the CaNNN assignment and is consistent with similar Ca–N force constants for $CaNH_2$ and CaN_3.

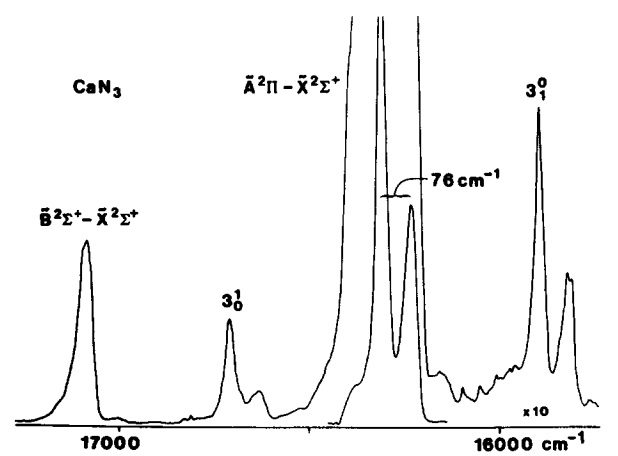

FIG. 3. Resolved fluorescence spectrum for CaN_3 recorded by exciting the $\Delta v = 0$ bands of the $\tilde{A}\,^2\Pi_{3/2}$–$\tilde{X}\,^2\Sigma^+$ system and dispersing the fluorescence with a monochromator. Significant relaxation to the $\tilde{A}\,^2\Pi_{1/2}$ and $\tilde{B}\,^2\Sigma^+$ states is apparent. The 3_1^0 and 3_0^1 bands are relatively strong, consistent with a Frank–Condon factor of about 0.07. In addition, several weak shoulders are interpreted as $2\nu_5$ in either the ground or excited states.

The other strong mode for these species is the metal-ligand bend (ν_5), but, for CaN_3, ν_5 has an extremely low frequency. Some of the shoulders on several bands are assigned to activity in the bending mode. Because ν_5 has π symmetry, we assign these peaks to two quanta and the bending frequency is found to be 43 cm^{-1} in the $\tilde{X}\,^2\Sigma^+$ state. ν_1 and ν_2, the azide antisymmetric and symmetric stretches, were also seen very weakly at 2114 cm^{-1} and 1364 cm^{-1}, respectively. These values are very similar to the frequencies in solid calcium azide, determined by Gray and Waddington,[17] of 2114 and 1380 cm^{-1}. The antisymmetric stretching frequency is, however, quite different from the value of 1986 cm^{-1} found by Polak *et al.*[23] for the free azide ion in the gas phase.

The spectrum of SrN_3 was also recorded. The low-resolution laser excitation scan is shown in Fig. 4. The curved baseline represents the signal due to scattered laser light and also indicates the variation in laser power across the scan. The SrN_3 spectrum is less clear than for CaN_3 (Fig. 2) and at first sight it appears to consist of a series of four equally spaced bands. This is because the 300 cm^{-1} spin–orbit splitting in the $\tilde{A}\,^2\Pi$ state matches the main vibrational frequency, the Sr–N stretch, and the spacing between the $\tilde{B}\,^2\Sigma^+$ state and the $\tilde{A}\,^2\Pi_{3/2}$ spin component is about 600 cm^{-1}. However, by comparison with CaN_3 and by recording resolved fluorescence with excitation of each band it was possible to assign the two red most peaks as the $\tilde{A}\,^2\Pi_{3/2}$–$\tilde{X}\,^2\Sigma^+$ and $\tilde{A}\,^2\Pi_{1/2}$–$\tilde{X}\,^2\Sigma^+$ origins while the blue most peak is the $\tilde{B}\,^2\Sigma^+$–$\tilde{X}\,^2\Sigma^+$ origin. The remaining peak is then due to overlapping vibrational bands of both the $\tilde{A}$–$\tilde{X}$ and $\tilde{B}$–$\tilde{X}$ systems. A summary of the observed band positions and vibrational frequencies for both CaN_3 and SrN_3 is provided in Table I.

TABLE I. Band origins for CaN_3 and SrN_3 (in cm^{-1}).

Transition	CaN_3	SrN_3
$\tilde{A}\,^2\Pi_{1/2}$–$\tilde{X}\,^2\Sigma^+$	16 217	14 933
$\tilde{A}\,^2\Pi_{3/2}$–$\tilde{X}\,^2\Sigma^+$	16 293	15 243
$\tilde{B}\,^2\Sigma^+$–$\tilde{X}\,^2\Sigma^+$	17 079	15 872

Vibrational frequencies (in cm^{-1})

Frequency	CaN_3 $\tilde{X}$	$\tilde{A}$	$\tilde{B}$
ν_1	2114		
ν_2	1364		
ν_3	396	389	384
$2\nu_5$	86		85
Frequency	**SrN_3 $\tilde{X}$**	**$\tilde{A}$**	**$\tilde{B}$**
ν_3	316	321	306
$2\nu_5$	82		

High-resolution analysis

In order to obtain information on the molecular structure of the azides, a rotational analysis of the 0–0 band of the $\tilde{A}\,^2\Pi$–$\tilde{X}\,^2\Sigma^+$ system of SrN_3 was carried out. The first problem was to determine the location of the 0–0 band. The low-resolution spectrum shown in Fig. 4 has some indication of bandhead structure, but no vibrational numbering is possible. To determine the position of the 0–0 band, the laser was scanned at high resolution (limited by the 0.03 cm^{-1} Doppler width of the lines) across the $\tilde{A}\,^2\Pi_{1/2}$–$\tilde{X}\,^2\Sigma^+$ band while the total fluorescence was monitored. A series of blue degraded bandheads were observed. On the long wavelength side of the band these formed a strong series separated by 7 cm^{-1}, as shown in Fig. 5. This series clearly came to an end, but one additional band was found 2.6 cm^{-1} lower in energy. Careful examination of the scan showed that this additional band was part of another series, also spaced by 7 cm^{-1}, but much weaker than the main series. The sequence bands involve the low frequency bending mode ν_5, which has a frequency of 43 cm^{-1} in the ground state. The sequence band spacing gives a value of 50 cm^{-1} for ν_5 in the $\tilde{A}\,^2\Pi$ state. This mode is doubly degenerate and exhibits a Renner–Teller interaction of the electronic and vibrational angular momenta in the $\tilde{A}\,^2\Pi$ state. The Renner–Teller effect leads to multiple bandheads for the higher sequence bands as can be seen in Fig. 5. The only vibrational level other than ν_5 likely to be populated at the effective molecular temperature of ~500 K is ν_3, the Sr–N stretch. The 3_1^1 band should be about a factor of 3 less intense than the origin band so the longest wavelength bandhead observed is assigned to 3_1^1 (Fig. 5).

The spectrum of SrN_3 is extremely dense because of the small rotational constant and the extensive sequence structure. The bandheads in Fig. 5 are superimposed on a strong background of weaker lines, none of which are resolved. In order to obtain single rotational lines from this dense spectrum, it is necessary to use the technique of laser excitation

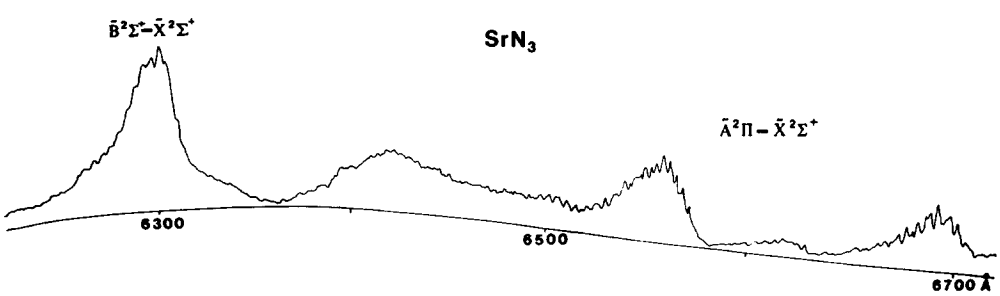

FIG. 4. Laser-induced fluorescence spectrum for SrN_3. The sloping baseline is due to the presence of scattered laser light and the shape of the curve represents the laser power curve. The $\tilde{A}\,^2\Pi$–$\tilde{X}\,^2\Sigma^+$ and $\tilde{B}\,^2\Sigma^+$–$\tilde{X}\,^2\Sigma^+$ systems of SrN_3 can be seen.

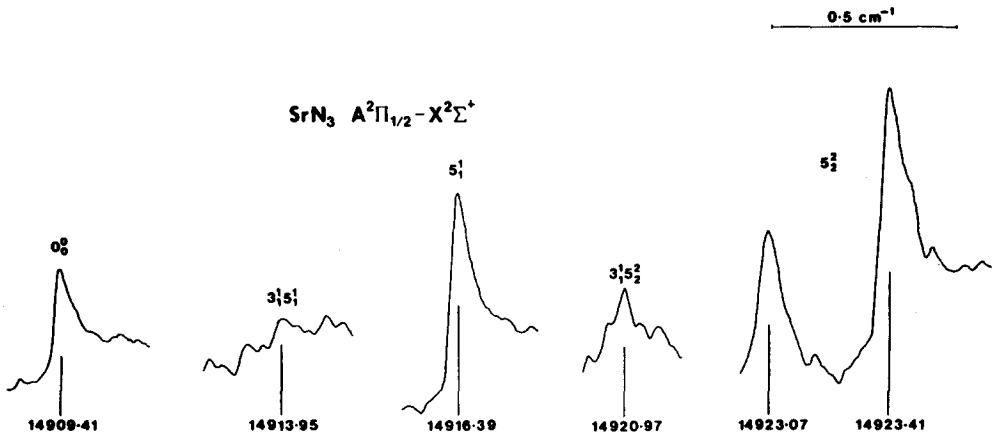

FIG. 5. Bandheads in the $\tilde{A}\,^2\Pi_{1/2}$–$\tilde{X}\,^2\Sigma^+$ system of SrN_3 recorded at Doppler-limited resolution. Note that there are large breaks between each segment of the spectrum. The vertical scale is the same for each peak, but the bandheads all have a large background signal subtracted from them. The unresolved background increases with increasing frequency because all of the bands are blue degraded. Two separate sequences in the Sr–N–N bending mode ν_5 can be seen, each sequence member spaced by 7 cm^{-1}. The strong sequence starts with the origin band while the weaker one involves the Sr–N stretch 3_1^1.

spectroscopy with selective fluorescence detection. The monochromator was set to record emission at the 0–0 bandhead and the laser was swept through several tens of wave numbers to pick up any lines connecting to the same upper state levels. The Hund's case (a) $^2\Pi$–Hund's case (b) $^2\Sigma^+$ nature of the transition results in six branches for each spin-component spaced approximately by $-3B$, $-B$, $+B$, and $+3B$ at low J with the $-B$ and $+B$ branches doubled due to the ground state spin-rotation interaction (see Herzberg[27] for a full description of a $^2\Pi$–$^2\Sigma^+$ transition). The $-B$ branches (P_{21} and Q_2 for $^2\Pi_{3/2}$–$^2\Sigma^+$) form the prominent bandheads (Fig. 5). Only the $+3B$ branch (R_1) connects to the same lambda doubling levels in the excited state as the P_1 and Q_{12} heads so only the R_1 branch was observed in the initial scan. Subsequently, the other branches were recorded in a similar fashion; for example, a section of the $+B$ (Q_{21} $+R_2$) branch recorded by monitoring $-3B$ (P_2) branch for $^2\Pi_{3/2}$–$^2\Sigma^+$ transition is shown in Fig. 6. The doubling due to the ground state spin–rotation interaction is apparent but is quite small ($\gamma = 4.86\times10^{-4}\,cm^{-1}$) and only becomes observable at about $N'' = 60$.

Rotational lines from 10 of the 12 possible branches of a $^2\Pi$–$^2\Sigma^+$ transition were recorded. Due to the extremely small rotation constant ($B'' = 0.045\,cm^{-1}$), the intensity of the rotational Boltzmann distribution peaks at about $N = 60$ for a temperature of 500 K and lines out to $N = 170$ were recorded. A total of 1169 lines were measured and these are given in Table II (see PAPS, Ref. 32), together with the residuals from the final fit. Standard energy level expressions were used for the $^2\Sigma^+$ state and the $\hat{N}^2$ formulation of the effective Hamiltonian of Brown *et al.*[28] was used for the $^2\Pi$ state. Explicit matrix elements are given by Amiot *et al.*[29]

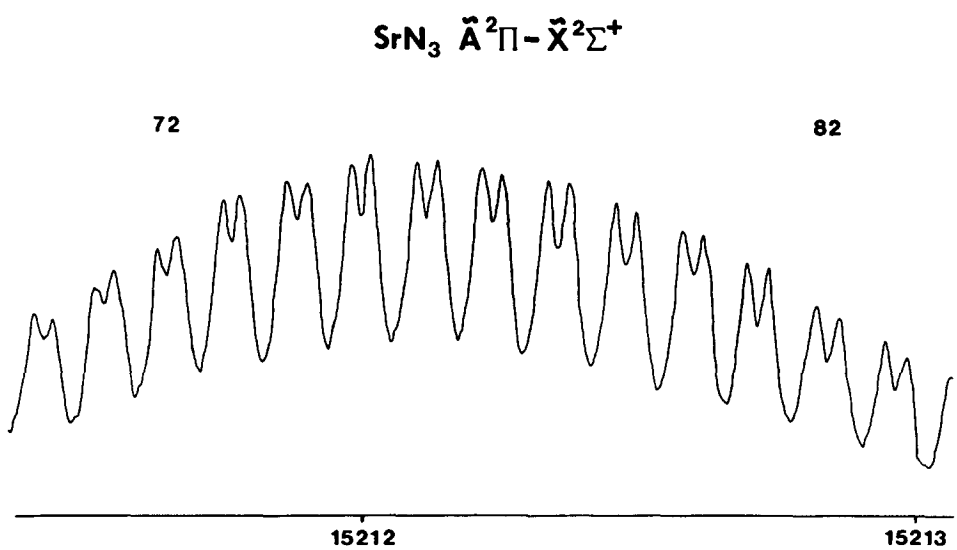

FIG. 6. Single rotational lines in the $+B$ branch of the $\tilde{A}\,^2\Pi_{3/2}$–$\tilde{X}\,^2\Sigma^+$ component recorded by scanning the single frequency laser and monitoring the fluorescence dispersed through a monochromator. The monochromator was set to record emission in the $-3B$ (P_2) branch near $N = 75$. The splitting is due to the ground state spin-rotation interaction and becomes apparent at about $N = 60$. The lower frequency component of the $+B$ pair of branches is Q_{21} and the upper one R_2 because the spin–rotation constant γ is positive in the $\tilde{X}\,^2\Sigma^+$ state.

The lines were fitted to their estimated experimental precision of 0.002 cm^{-1} with the 12 constants given in Table III. The inclusion of the distortion parameters γ_D and p_D was required because of the high rotational levels probed. The data could be fitted reasonably well without these two parameters, but small systematic residuals were observed.

The spin–orbit constant in the $\tilde{A}\,^2\Pi$ state is significantly larger (296 cm^{-1}) than in the previously observed oxygen bonded species, for example, $A = 264$ cm^{-1} for SrOH and $A = 267$ cm^{-1} for $SrOCH_3$. This suggests that the N_3^- ligand significantly changes the shape of the molecular orbitals centered on Sr^+ from the shapes produced by the OH^- and CH_3O^- ligands. The lambda doubling parameters can be estimated assuming a pure-precession interaction with the $\tilde{B}\,^2\Sigma^+$ state. The value for p (Ref. 30) is given by

$$p = \frac{2ABl(l+1)}{E(\tilde{A}\,^2\Pi) - E(\tilde{B}\,^2\Sigma^+)}$$

is -0.0686 cm^{-1} for $l = 1$. The experimental value is $-0.058\,69$ cm^{-1} in reasonable agreement. The value for q given by

$$q = \frac{2B^2l(l+1)}{E(\tilde{A}\,^2\Pi) - E(\tilde{B}\,^2\Sigma^+)}$$

is -10.5×10^{-6} cm^{-1} compared to the experimental value of -6.7×15^{-6} cm^{-1}. These expressions should not be taken too seriously, but they do indicate that the $\tilde{B}\,^2\Sigma^+$ and $\tilde{A}\,^2\Pi$ states of SrN_3 have substantial $5p$ and $4d$ Sr^+ character. A similar expression for p_D (Ref. 31) gives

$$p_D = \frac{-2pD}{B} = 8.6\times10^{-9}\ cm^{-1}$$

compared to the experimental value of 4.5×10^{-9} cm^{-1}.

Only one rotational constant was determined, but there are three structural parameters for SrN_3. To determine a value for the Sr–N bond length, the two N–N distances were fixed at 1.18 Å from the crystal structure.[18] The recent high-resolution analysis of Polak *et al.*[23] gives 1.188 Å for the N–N bond length in N_3^-, but in view of the lower frequency observed for the antisymmetric stretching vibration, it was considered more appropriate to use the crystal value.

This yields an r_0 value for the Sr–N bond length of 2.262 Å. The corresponding value for $Sr–NH_2$ was 2.254 Å showing that the bonding in SrN_3 is very similar to that in $SrNH_2$.

TABLE III. Molecular constants for 0–0 band of the $\tilde{A}\,^2\Pi$–$\tilde{X}\,^2\Sigma^+$ transition of SrN_3 (in cm^{-1}).

$\tilde{X}\,^2\Sigma^+$
$B = 0.044\,863\,5(13)$[a]
$D = 3.458(50)\times10^{-9}$
$\gamma = 4.857(47)\times10^{-4}$
$\gamma_D = 1.16(26)\times10^{-9}$
$\tilde{A}\,^2\Pi$
$T_{00} = 15\,057.692\,9(1)$
$A = 296.431\,71(22)$
$A_D = -5.637(25)\times10^{-6}$
$B = 0.045\,331\,2(12)$
$D = 3.320(49)\times10^{-9}$
$q = -6.74(63)\times10^{-6}$
$p = -0.058\,691\,6(76)$
$p_D = 4.51(66)\times10^{-9}$

[a]Values in parentheses are one standard deviation errors from the least squares fit.

CONCLUSION

The first high-resolution spectrum of a metal azide molecule has been detected by laser excitation spectroscopy. The CaN_3 and SrN_3 free radicals have linear geometries and SrN_3 has a Sr–N bond length of 2.26 Å.

ACKNOWLEDGMENTS

This research was supported by the National Science Foundation (NSF-8608630). Partial support was also provided by the Office of Naval Research.

[1]P. F. Bernath and S. Kinsey-Nielsen, Chem. Phys. Lett. **105**, 663 (1984).
[2]P. F. Bernath and C. R. Brazier, Astrophys. J. **288**, 373 (1985).
[3]C. R. Brazier and P. F. Bernath, J. Mol. Spectrosc. **114**, 163 (1985).
[4]A. M. R. P. Bopegedera, C. R. Brazier, and P. F. Bernath, J. Phys. Chem. **91**, 2779 (1987).
[5]C. R. Brazier and P. F. Bernath (in preparation).
[6]C. R. Brazier and P. F. Bernath, J. Chem. Phys. **86**, 5918 (1987).
[7]L. C. Ellingboe, A. M. R. P. Bopegedera, C. R. Brazier, and P. F. Bernath, Chem. Phys. Lett. **126**, 285 (1986).
[8]L. C. O'Brien and P. F. Bernath, J. Chem. Phys. **88**, 2117 (1988).
[9]M. H. V. Douay and P. F. Bernath (in progress).
[10]S. Patai, *The Chemistry of the Azide Group* (Interscience, London, 1971).
[11]A. M. Golub, H. Kohler, and V. V. Skopenko, *Chemistry of Pseudohalides* (Elsevier, Amsterdam, 1986).
[12]*Energetic Materials*, Vol. 1, edited by H. D. Fair and R. F. Walker (Plenum, New York, 1977).
[13]F. C. Tompkins and D. A. Young, Discuss. Faraday Soc. **23**, 202 (1957).
[14]F. C. Tompkins and D. A. Young, Trans. Faraday Soc. **61**, 1470 (1965).
[15]E. G. Prout and E. G. Shephard, J. Inorg. Nucl. Chem. **43**, 1977 (1981).
[16]R. J. Colton and J. W. Rabalais, J. Chem. Phys. **64**, 3481 (1976).
[17]P. Gray and T. C. Waddington, Trans. Faraday Soc. **53**, 901 (1957).
[18]G. E. Pringle and D. E. Noakes, Acta Crystallogr. Sect. B **24**, 262 (1968).
[19]Von H. Krischner and G. Kelz, Z. Anorg. Allg. Chem. **494**, 203 (1982).
[20]R. L. Jackson, M. J. Pellerite, and J. I. Brauman, J. Am. Chem. Soc. **103**, 1802 (1981).
[21]E. Illenberger, P. B. Comita, J. I. Brauman, H.-P. Fenzlaff, M. Heni, N. Heinrich, W. Koch, and G. Frenking, Ber. Bunsenges. Phys. Chem. **89**, 1026 (1985).
[22]P. Botschwina, J. Chem. Phys. **85**, 4591 (1986).
[23]M. Polak, M. Gruebele, and R. J. Saykally, J. Am. Chem. Soc. **109**, 2884 (1987).
[24]J. B. West, R. S. Bradford, J. D. Eversole, and C. R. Jones, Rev. Sci. Instrum. **46**, 164 (1975).
[25]P. Gunther, R. Meyer, and F. Müller-Skjold, Z. Phys. Chem. A **175**, 154 (1935).
[26]R. C. Hilborn, Q. Zhu, and D. O. Harris, J. Mol. Spectrosc. **97**, 73 (1983).
[27]G. Herzberg, *Spectra of Diatomic Molecules*, 2nd ed. (Van Nostrand-Reinhold, New York, 1950), p. 257.
[28]J. M. Brown, E. A. Colbourn, J. K. G. Watson, and F. D. Wayne, J. Mol. Spectrosc. **74**, 294 (1979).
[29]C. Amiot, J. P. Maillard, and J. Chauville, J. Mol. Spectrosc. **87**, 196 (1981).
[30]R. S. Mulliken and A. Christy, Phys. Rev. **38**, 87 (1931).
[31]L. Veseth, J. Phys. B **3**, 1677 (1970).
[32]See AIP document no. PAPS JCPSA-88-2112-11 for 11 pages of Table II (observed lines of the $\tilde{A}\,^2\Pi$–$\tilde{X}\,^2\Sigma^+$ system of SrN_3). Order by PAPS number and journal reference from American Institute of Physics, Physics Auxiliary Publication Service, 335 East 45th Street, New York, NY, 10017. The price is $1.50 for each microfiche (98 pages) or $5.00 for photocopies of up to 30 pages, and $0.15 for each additional page over 30 pages. Airmail additional. Make checks payable to the American Institute of Physics.